

Attaining near-optimal Dicke superradiance in a large spatial scale

Jun Ren^{1,2,*}, Shicheng Zhu², and Z. D. Wang^{1†}

¹ Guangdong-Hong Kong Joint Laboratory of Quantum Matter,

Department of Physics, and HK Institute of Quantum Science & Technology,

The University of Hong Kong, Pokfulam Road, Hong Kong, People's Republic of China

² College of Physics and Hebei Key Laboratory of Photophysics Research and Application, Hebei Normal University, Shijiazhuang, Hebei 050024, People's Republic of China

Dicke superradiance is the first example for collective emission that is the hallmark of light-matter interaction. Superradiance for arrays of inverted emitters in free space only survives at tiny emitter-to-emitter distances and requires interactions beyond the nearest-neighbor. Epsilon-near-zero (ENZ) materials are natural mediators for long-range interactions because of their infinite effective wavelengths. We study the superradiance properties in two types of ENZ structures, plasmonic waveguide and dielectric photonic crystal, and show that ENZ materials have great potential to realize spatially extended and near-optimal Dicke superradiance. We perform this by applying the method we derived to determine the occurrence of superradiance that is applicable to complex coupling cases. Additionally, we determine the role of quantum coherence in collective emission dynamics for the case of all-to-all interaction by numerically analyzing the emission dynamics of a few-emitter system. We also show that the maximum quantum coherence in the system can be determined using the maximum photon burst rate. The findings of this paper have prospective applications in quantum information processing and light-matter interaction, and they can be implemented by current experiments.

I. INTRODUCTION

The original Dicke superradiance is referred to as the phenomenon that N inverted emitters with identical interactions lock in phase and emit photons in a short time with intensity scales as N^2 [1–3], giving rise to emission burst. Due to its wide applications in single-photon source [4, 5], light harvesting [6–8], quantum information [4, 9–11], etc., in recent years, superradiance has made a lot of progress in various platforms, such as ion traps [12, 13], Rydberg gases [14–16], and superconducting systems [17–20]. The ideal Dicke superradiance assumes that a large amount of emitters are confined in a compact region with a linear dimension significantly smaller than the emission wavelength λ . Therefore, the emitters are indistinguishable when they absorb or emit a photon, making their quantum state a Dicke state, which can reduce the 2^N -dimensional Hilbert space to $N + 1$ dimensions. The polynomial complexity superradiance scenario has been expanded by recent theoretical studies to spatially extended and ordered atomic chains [29–31] and arrays [33–36, 40]. Furthermore, it has been demonstrated that the eigenvalues of a N -dimensional decoherence matrix, whose elements are the incoherent emitter-emitter coupling (also known as dissipative coupling in certain literature), are the key element of the minimal condition of superradiance.

The superradiance of the ordered atomic array in free space, where the interactions between emitters decrease exponentially with the emitter-emitter distance, is the subject of the majority of existing theories. This, however, severely reduces the range of scenarios where the superradiance theory can be applied, since in many cases, non-uniform amplitude and phase of the electromagnetic field around emitters results in ir-

regular emitter-emitter couplings and inhomogeneous single-emitter emission rates. Furthermore, in free space, a superradiance burst survives only when the emitter-emitter distance is small enough, even for a very short chain [29]. It has been shown in Ref. [35] that, superradiance has a minimum requirement, and the authors provided a maximal inter-atomic separation at which superradiance for uniform atomic arrays can be observed. Superradiance cannot happen with just nearest-neighbor atomic interaction, according to a fairly recent research [37]. This significantly reduces the spatial scale of superradiant emitters.

Therefore, on the one hand, a more general theory that can be used to assess the existence of superradiance in more complicated scenarios and that only requires the N -dimensional decoherence matrix would be helpful. On the other hand, it is observed that the two main ingredients needed to realize superradiance at large spatial scale are long-range and large dissipative interactions between distant emitters. Plasmonic or photonic waveguides appear to be good mediators for long-distance interactions and thus superradiance [21–26, 28, 47, 48]. Nevertheless, these systems often have tight requirements about the position of the emitters. Due to their infinite wavelength and vanishingly small index, recent advancements in near-zero-index (NZI) materials, such as plasmonic epsilon-near-zero (ENZ) waveguides and all-dielectric ENZ photonic crystals, eliminate this drawback [42–46]. As a result, they can attain all-to-all interactions and thus near-optimal Dicke superradiance in extended space. Moreover, it is interesting to explore the role of quantum resource in emission dynamics and elucidate the intrinsic connection between quantum resource and collective emission.

In this work, we develop a universal criterion for determining whether superradiance occurs, which only requires dealing with the N -dimensional decoherence matrix, rather than computing emission dynamics that grows exponentially with emitter number N . We apply this theory to two ENZ systems that can acquire long-range emitter-emitter couplings, plas-

* renjun@hebtu.edu.cn

† zwang@hku.hk

monic waveguide and dielectric photonic crystal, and demonstrate that both structures support near-optimal Dicke superradiance in an extended space. Moreover, we numerically calculate the dynamics of a few-emitter system in all-to-all case, and divide the dynamics into two parts, single-emitter emission and collective emission. We figure out that the dynamics of quantum coherence is completely synchronous with the collective emission part, and there is an exact correspondence between maximum quantum coherence and maximum emission rate of superradiance, making superradiance emission rate a possible measurement tool for quantum coherence.

The paper is organized as follows: In Section II, we derive the minimal condition for superradiance that only require dealing with the N -dimensional decoherence matrix, and examine the relationship between the maximum emission rate and second-order correlation function. In Section III, using two ENZ materials, namely the plasmonic waveguide and the dielectric photonic crystal, we demonstrate that achieving near-optimal superradiance for multiple emitters is possible in an extended spatial domain. In Section IV, we discuss the role of quantum coherence in emission dynamics of all-inverted emitters in the all-to-all scenario. We find that the quantum coherence is synchronous with the collective emission, but after the collective emission ends, the quantum coherence even be detrimental to total emission. In Section V we finally conclude.

II. PHOTON EMISSION OF IDENTICAL EMITTERS AT EARLY TIME

In the study of the dynamic evolution of multi-emitter system in a weakly coupled environment, Born-Markov and rotating-wave approximations can be used. After tracing out the environment, the Lindblad master equation of emitter system can be written as [26, 49, 50]

$$\frac{\partial \rho}{\partial t} = \frac{i}{\hbar} [\rho, H] + \frac{1}{2} \sum_{i,j} \gamma_{ij} \left(2\sigma_i \rho \sigma_j^\dagger - \rho \sigma_i^\dagger \sigma_j - \sigma_i^\dagger \sigma_j \rho \right), \quad (1)$$

where σ_i^\dagger and σ_i are the raising and lowering operators of the i th emitter, respectively. The γ_{ij} is the incoherent coupling between the i th and j th emitters, and all the γ_{ij} s together will be shown to control the emission process of multi-emitter system. The Hamiltonian of the emitter system is

$$H = \hbar\omega_0 \sum_i \sigma_i^\dagger \sigma_i + \sum_{i \neq j} g_{ij} \sigma_i^\dagger \sigma_j, \quad (2)$$

with ω_0 being the transition frequency of the two-level emitters. The coherent coupling strength g_{ij} has been shown to have a small impact on emission dynamic [35]. In Eq. (1), ρ is the density matrix of the emitter system, $[\rho, H]$ and Lindblad term [the second term of the right-hand side of Eq. (1)] govern the coherent and incoherent parts of the emitter dynamics, respectively.

Under the point dipole approximation, the coherent and incoherent interactions between the i th and j th emitters g_{ij} and

γ_{ij} can be written as [49]

$$g_{ij} = \frac{\omega_0^2}{\varepsilon_0 \hbar c^2} \text{Re} \left[\vec{\mu}_i^* \cdot \overset{\leftrightarrow}{G}(\vec{r}_i, \vec{r}_j, \omega) \cdot \vec{\mu}_j \right] \quad (3)$$

and

$$\gamma_{ij} = \frac{2\omega_0^2}{\varepsilon_0 \hbar c^2} \text{Im} \left[\vec{\mu}_i^* \cdot \overset{\leftrightarrow}{G}(\vec{r}_i, \vec{r}_j, \omega) \cdot \vec{\mu}_j \right], \quad (4)$$

respectively. The $\vec{\mu}_i$ and $\vec{\mu}_j$ are the dipole moments of the i th and j th emitters, and the detailed calculation of the electric Green's tensor $\overset{\leftrightarrow}{G}$ can be found in Sec. III.

The total emission rate of the emitter system at time t can be written as

$$\gamma(t) = \gamma_s(t) + \gamma_c(t), \quad (5)$$

where we define

$$\gamma_s(t) \equiv \sum_j \gamma_{jj} \langle \hat{e}_j \rangle \quad (6)$$

that governs the emission rate from single emitters, which originates from the diagonal elements of the density matrix $\rho(t)$ and decays exponentially, and

$$\gamma_c(t) \equiv \sum_{i \neq j} \gamma_{ij} \langle \hat{\sigma}_i^\dagger \hat{\sigma}_j \rangle \quad (7)$$

governs the collective emission, which causes the correlation-induced emission and originates from the non-diagonal elements of density matrix. The operators in Eqs. (6) and (7) are $\hat{e}_j \equiv |e_j\rangle\langle e_j|$, $\hat{\sigma}_j \equiv |g_j\rangle\langle e_j|$, and $\hat{\sigma}_j^\dagger \equiv |e_j\rangle\langle g_j|$, with $|e_j\rangle$ and $|g_j\rangle$ being the upper and lower energy levels of the j th emitter. Studying the single-emitter and collective emission dynamics independently can help us understand their roles in the overall emission process and how they relate to the superradiance and quantum resources in the system, as we can see in Sec. IV.

Therefore, the superradiance occurs only when the increase rate of the total emission rate is larger than zero at the beginning of the emission, that is the first derivative $\dot{\gamma}(0) > 0$. According to Refs. [40, 41], if the emitters are fully inverted initially, namely $|\psi(0)\rangle = |e\rangle^{\otimes N}$, the derivative of $\langle \hat{e}_j \rangle$ and $\langle \hat{\sigma}_i^\dagger \hat{\sigma}_j \rangle$ at $t = 0$ can be calculated as

$$\frac{d\langle \hat{e}_j \rangle}{dt}(0) = -\gamma_{jj}, \quad \frac{d\langle \hat{\sigma}_i^\dagger \hat{\sigma}_j \rangle}{dt}(0) = \gamma_{ij}. \quad (8)$$

Substituting Eq. (8) into the first derivative of Eq. (5), we have

$$\dot{\gamma}(0) = -\sum_j \gamma_{jj}^2 + \sum_{i \neq j} \gamma_{ij}^2. \quad (9)$$

From Eqs. (8) and (9) it can be inferred that the non-diagonal elements of the decoherence matrix Γ contribute to the superradiance whereas the diagonal elements do the opposite. The competition between them determines whether or not the superradiance occurs. If we set the decoherence matrix

$\mathbf{\Gamma} = (\gamma_{ij})$ with the matrix elements γ_{ij} being defined in Eq. (4), the $\dot{\gamma}(0)$ can be written as a compact form

$$\dot{\gamma}(0) = \text{Tr}(\mathbf{\Gamma}^2) - 2\text{Tr}(\mathbf{\Gamma}_d^2), \quad (10)$$

where $\mathbf{\Gamma}_d \equiv \text{diag}(\gamma_{11}, \gamma_{22}, \dots, \gamma_{NN})$ is the diagonal matrix of $\mathbf{\Gamma}$. Consequently, the superradiance criterion $\dot{\gamma}(0) > 0$ can be used to determine the minimal requirement for superradiance, which can be derived as

$$\text{Tr}(\mathbf{\Gamma}^2) > 2\text{Tr}(\mathbf{\Gamma}_d^2). \quad (11)$$

Here, it can be observed that superradiance in an all-inverted multi-emitter system can be determined without the need for dipole-dipole coupling [as shown in Eq. (3)]. Therefore, we can state that whether superradiance occurs is independent with the coherent coupling between emitters. However, it should be pointed out that this does not imply that coherent coupling has no effect on the emission dynamics process. Because the first derivatives of the expected values of the two operators shown in Eq. (8) are decoupled only at the initial moment of emission, but are coupled with each other at all subsequent times, see Refs. [40, 41].

Recent research [29–31, 35] suggests that superradiance may be seen as the first emitting photon enhancing the rate of the second one. This interpretation is based on the jump operator profile. In order to ascertain if superradiance occurs, they defined an easily computed second-order correlation function $g^{(2)}(0)$ of identical emitters at the beginning of the emission. Without assuming anything about the emitters' environment, we find that $g^{(2)}(0)$ can be calculated as

$$g^{(2)}(0) = 1 + \frac{\text{Tr}(\mathbf{\Gamma}^2) - 2\text{Tr}(\mathbf{\Gamma}_d^2)}{(\text{Tr}\mathbf{\Gamma})^2}, \quad (12)$$

in which the meaning of $\mathbf{\Gamma}$ and $\mathbf{\Gamma}_d$ are identical to those in Eq. (10). The detailed procedure of jump operation method and the derivation of Eq. (12) can be found in the Supplemental Material. Therefore, it is easy to find that the minimal superradiance condition of $g^{(2)}(0) > 1$ is consistent with the condition indicated in Eq. (11) we obtained. Since $g^{(2)}(0)$ has a value range of 0 to 2, as can be seen below, and because there is frequently a definite positive connection between it and the emission rate, we use it to determine the occurrence of the superradiance in this work.

Keep in mind that, other from assuming that all emitters are identical and have the same transition frequency, we made no further assumptions while deriving the superradiance condition above. This result is important for those situations where emitters are in a complex environment rather than homogeneous free space, such as the plasmonic systems [21–23], where the decay and interaction are sensitive to the spatial arrangement of emitters, and these systems are frequently used to increase the emission rate of collective emitter systems. Therefore, as long as their decoherence matrix $\mathbf{\Gamma}$ is known, the result of Eqs. (10)–(12) is can be used to assess whether a multi-emitter system will undergo superradiance in general, and the dynamics of the whole 2^N -dimensional system does not need to be calculated. Furthermore, as shown in Sec. IV,

$g^{(2)}(0)$ has an extensive connection with the emission dynamics, it is also possible to calculate this value in order to assess the emission characteristics for a large number of emitters.

Next, we examine the initial second-order correlation function in several special cases. The first involves identical spontaneous decay but distinct emitter-emitter couplings. According to Cauchy-Schwarz inequality, we have

$$\left(\sum_{i=1}^N \gamma_{ii}\right)^2 \leq N \left(\sum_{i=1}^N \gamma_{ii}^2\right), \quad (13)$$

where the equality is taken if and only if all the diagonal elements γ_{ii} are equal, we set $\gamma_{ii} = \gamma_0$, and along with Eq. (10) we have

$$g^{(2)}(0) \leq 1 + \frac{\text{Tr}(\mathbf{\Gamma}^2)}{(\text{Tr}\mathbf{\Gamma})^2} - \frac{2}{N}, \quad (14)$$

where the equality is taken if and only if every emitter is in the same electromagnetic environment, resulting in an identical spontaneous decay rate. The right-hand side of Eq. (14) is the same as in the existing results [31, 35], where the free-space environment is assumed. As indicated in Ref. [35], for a constant emitter number N , the $g^{(2)}(0)$ is proportional to the variance of the eigenvalues of matrix $\mathbf{\Gamma}$ when the single emitter emission rate is identical. However, when the emitters' decay rates diverge, as illustrated in the Supplemental Material, this criterion is violated.

The second special case is the identical spontaneous decay and emitter-emitter coupling. We refer to this scenario as an all-to-all interaction since any two emitters will interact in the same way. We now assume that the emitters' spontaneous decay rates are equal since the amplitude of electric field in the emitter's region is uniform. Furthermore, we also assume that the phase of electric field keeps invariant in space and thus the dissipative couplings are also identical, but less than 1. If we set the coupling between any two emitters as α ($\alpha < 1$), the normalized dissipative matrix has the form of

$$\mathbf{\Gamma} = \begin{pmatrix} 1 & \alpha & \cdots & \alpha \\ \alpha & 1 & \cdots & \alpha \\ \vdots & \vdots & \ddots & \vdots \\ \alpha & \alpha & \cdots & 1 \end{pmatrix}, \quad (15)$$

and according to Eq. (12) the second-order function at the initial time $g^{(2)}(0)$ can be calculated as

$$g^{(2)}(0) = \frac{N-1}{N}(1+\alpha^2). \quad (16)$$

To satisfy the superradiance criterion $g^{(2)}(0) > 1$ in this scenario, α needs to be greater than $1/\sqrt{N-1}$ for a given N . Of course, this condition is readily met when N is very large, and the actual challenge is in achieving the all-to-all interaction in practical scenarios. In Sec. III, we will go through in detail how to create this almost perfect all-to-all interaction situation.

When superradiance occurs, there are two important characteristic indices for the emission dynamics, the time t_m when

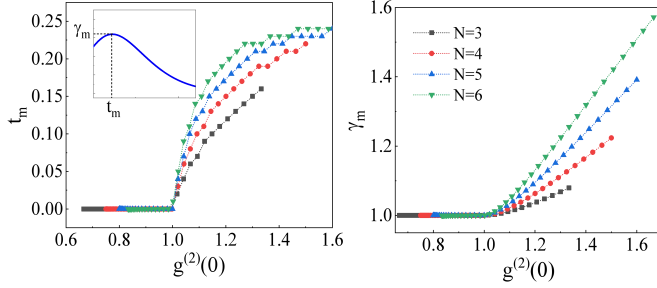


FIG. 1. (Color online) Relationship between maximum emission rate t_m (a), its corresponding time γ_m (b) with the second-order correlation $g^{(2)}(0)$ under different emitter number N . Inset: A schematic diagram of the relationship between the emission rate of superradiance and time.

the total emission rate $\gamma(t)$ reaches the maximum value, and the corresponding emission rate γ_m , as shown in the inset in Fig. 1(a). The larger the γ_m , the greater the intensity of radiation when the superradiance burst occurs. It is well known that, when the number of emitters is large, it is difficult to numerically solve their dynamic evolution. Therefore, it would be of great significance if we could characterize the superradiance properties using $g^{(2)}(0)$ as shown in Eq. (12), which is very easy to obtain as long as the matrix Γ is known.

Ref. [35] discussed in detail how the superradiance properties of emitter arrays of different dimensions in free space change with the emitter-emitter distance. Here, by solving the dynamic evolution of the few-emitter system shown in Eq. (1), we extract the maximum total emission rate γ_m and the corresponding time t_m in the case of all-to-all interactions [i.e., the decoherence matrix is represented in Eq. (15)], and plot their relationship with the second-order correlation function $g^{(2)}(0)$, as shown in Fig. 1. Different curves in Figs. 1 (a) and 1(b) respectively represent the relationship between t_m , γ_m and the second-order correlation $g^{(2)}(0)$ under different emitter number N . Different $g^{(2)}(0)$ in the same curve is realized by changing the parameter α in Eq. (15) from 0 to 1.

As illustrated in Fig. 1, when $g^{(2)}(0)$ is less than 1, superradiance will not occur. In this case, the emission rate decays exponentially with time, so t_m is always 0 and γ_m is always 1 (all the emission rates in this work are normalized by $\text{tr}(\Gamma)$). As $g^{(2)}(0)$ exceeds 1, t_m begins to be greater than 0, and γ_m begins to be greater than 1, which means superradiance occurs. As $g^{(2)}(0)$ further increases, for a fixed N , both t_m and γ_m gradually increase. For the γ_m , the relationship between it and the $g^{(2)}(0)$ is roughly linear when $g^{(2)}(0)$ is large.

The results in Fig. 1 have many-fold meanings for the all-to-all case. On the one hand, it verifies that $g^{(2)}(0) > 1$ is a necessary and sufficient condition to indicate superradiance (this determination of sufficiency and necessity holds true for any complex emitter environment, which can be determined by taking a large number of random decoherence matrices and is not shown here). On the other hand, it points out how to efficiently increase the intensity of superradiance emission in the case of all-to-all interaction, that is, increase the number of emitters or enhance the incoherent coupling α . Moreover,

we can observe that when $g^{(2)}(0)$ is large enough, there is almost a linear relationship between maximum emission rate γ_m and $g^{(2)}(0)$. And as N increases, the slope of the straight line also increases. Therefore, the results in Fig. 1 can be used to approximately predict the maximum emission rate when N is very large.

III. ATTAINING LARGE SUPERRADIANCE USING ENZ STRUCTURES

As indicated in Refs. [29, 31, 35], superradiance cannot occur with only nearest-neighbor coupling, and the longer the interaction range, the larger the correlation $g^{(2)}(0)$ and the emission intensity. Therefore, to reach large $g^{(2)}(0)$, we need to build a system of long-distance interacting emitters in order to pursue increasing emission intensity. This all-to-all interaction cannot be achieved in free space unless the density of emitters increases to infinity, as we know that the coupling between regularly arranged emitter arrays in free space rapidly decays with increasing distance.

In recent years, the emergence of NZI materials [42–46] has made this all-to-all interaction scenario possible. Among NZI materials, ENZ structures have drawn a lot of attention because they support infinitely long effective wavelengths without altering the phase of the electric field in space. Owing to this remarkable characteristic, emitters in these systems are increasingly focusing on long-range [47] and location-insensitive interactions [48]. In this section, we focus on the superradiance properties of two popular ENZ structures: the plasmonic ENZ waveguide and the dielectric ENZ photonic crystal.

A. Superradiance of emitters in plasmonic ENZ waveguides

In the spatial scale range of hundreds of nanometers, the ENZ waveguide naturally provides a uniform dissipative coupling between any two emitters. The periodic-arranged slit waveguide cell (with grating period $a = b = 400$ nm) is shown in the upper panel of Fig. 2(a). The medium surrounding the slit is the metal Ag, whose permittivity is adapted from experiment [51]. The slit is composed of dielectric material with permittivity $\epsilon = 2.2$. The emitters are inserted in the central line of the waveguide, as shown in the panel, where the arrows represent the orientation of the dipole moment of emitters. The slit length, width and height are taken as $l = 1$ μm , $w = 200$ nm, and $h = 40$ nm, respectively.

In this work, we set all the dipole moments of emitters along the y -axis. According to Refs. [52, 53], the effective refractive index can be calculated using the dispersion equation of a rectangular waveguide, because the modal distribution of present waveguide is very similar to that of quasi-TE₁₀ mode [52]. The real and imaginary parts of the effective index n_{eff} are presented in Fig. 2(b) with solid and dashed lines, respectively. The near-zero index can be observed in the frequency range from 290 to 300 THz. This near-zero index has great potential in achieving long-range interaction between emitters and thus emission burst as described in Sec. II. At

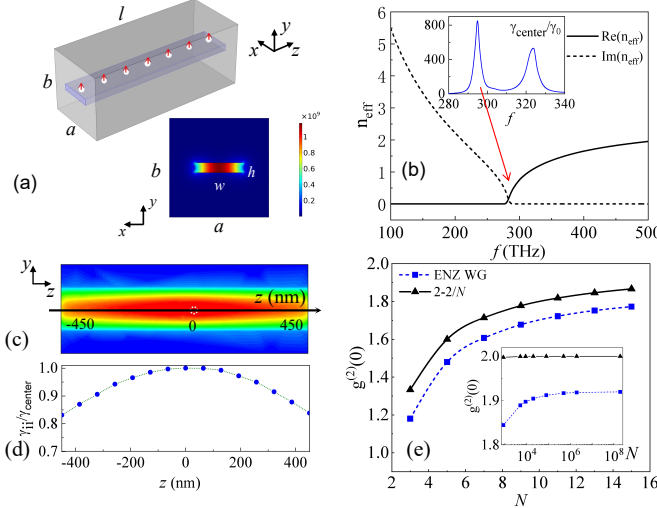


FIG. 2. (Color online) (a) Upper panel: Schematic diagram of an ENZ waveguide and the emitters inserted in it. Lower panel: The field pattern in the $x-y$ plane of a central emitter with ENZ transition frequency $f = 295$ THz. (b) Effective refractive index in the slit as a function of frequency. Inset: The enhancement of single-emitter spontaneous decay rate as a function of frequency. (c) The field distribution in the $y-z$ plane of a single emitter located at the center of the slit with $f = 295$ THz. (d) The normalized spontaneous decay rate of an emitter chain in the central line of the waveguide. (e) The dependence of the calculated second-order correlation function $g^{(2)}(0)$ on the emitter number N .

the same time, the emission intensity is proportional to the decay rate of a single emitter. In the inset of Fig. 2(b), we plot the enhancement of spontaneous decay of a single emitter located in the center of the slit waveguide, $\gamma_{\text{center}}/\gamma_0$, with γ_0 being the spontaneous decay rate of the emitter in vacuum. Obviously, this single-emitter decay rate has a sharp peak around the frequency $f = 295$ THz, with a more than 800-fold enhancement compared to free space. Therefore, the large spontaneous emission rate and near-zero index make the ENZ waveguide an excellent candidate for achieving photon emission burst.

Here we first briefly describe how to calculate the dissipative coupling parameters γ_{ij} that are necessary for the superradiance indicator $g^{(2)}(0)$. It can be observed that the key to calculate the two parameters is calculating Green's tensor, according to Eq. (4). For the identical orientation of the dipole moments of emitters, the Green's function $\vec{G}(\vec{r}_i, \vec{r}_j, \omega)$ can be solved by calculating the electric field emitted by a dipole located at \vec{r}_j , i.e.

$$\vec{G}(\vec{r}_i, \vec{r}_j, \omega) \cdot \vec{\mu}_j = -\vec{E}_i(\vec{r}_i)_{\vec{r}_j}, \quad (17)$$

where $\vec{E}_i(\vec{r}_i)_{\vec{r}_j}$ is the electric field component along the orientation of the dipole moment of the i th emitter located at $\vec{r} = \vec{r}_i$, which is emitted from the j th emitter. For the single-emitter spontaneous decay rate γ_{ii} , we only need to calculate the electric field it feels by emitting from itself.

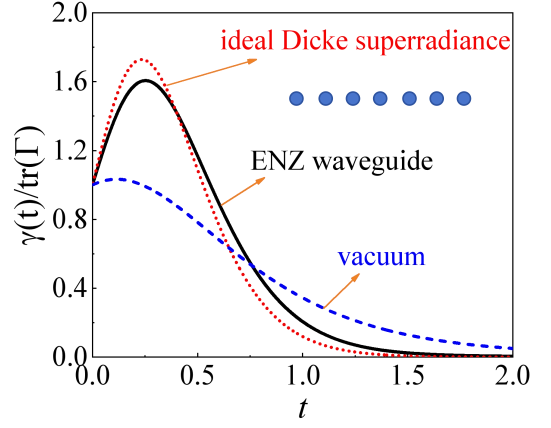


FIG. 3. (Color online) Total normalized emission rate $\gamma(t)/\text{tr}(\Gamma)$ versus time t with three cases: The 7 emitters are in a line in the ENZ waveguide (black solid line), idea Dicke superradiance (red dotted line), and in the vacuum (blue dashed line). The emitters have the same spatial arrangement in three cases, as indicated in the inset.

In the lower panel of Fig. 2(a) and Fig. 2(c), we present the amplitude of electric field of a dipole with transition frequency $f = 295$ THz located at the center of the slit in the $x-y$ and $y-z$ planes, respectively, and all the electric field simulations in this work (except for the vacuum case, which is readily at hand with the analytic formula) are performed using COMSOL multiphysics. The black arrow in Fig. 2(c) represents the line where the emitters are located, and the range of z -axis is from -450 to 450 nm. According to the two field patterns we know that, the field emitted from the center emitter distributed almost uniformly, especially near the central line of the slit waveguide. Even though, it is obvious that there is a decrease from the center of the slit to both sides of the waveguide. Therefore, naturally, when the emitters are lined up on the central axis of the slit [as shown in the upper panel of Fig. 2(a)], the spontaneous emission rates of emitters at different positions will be different. We plot the relationship between the normalized spontaneous emission rate of emitters and their positions (represented by z) in Fig. 2(d). It can be seen from the figure that the spontaneous emission rate of emitters gradually and symmetrically decreases from the center to both ends, reducing to about 80% of the center at the location of -450 or 450 nm. For comparison, for other frequencies (non-ENZ frequencies), the single-emitter decay rate will oscillate violently with the emitter position. The data the frequency $f = 324$ THz corresponding to the second resonance peak in the inset shown in Fig. 2(b) can be found in the Supplemental Material.

To calculate the correlation function $g^{(2)}(0)$ to judge whether the superradiance occurs or not, we can use Eq. (12) for all the coupling cases. The blue square-dashed line in Fig. 2(e) shows the dependence between the $g^{(2)}(0)$ of uniformly arranged emitters and the number of emitters N that we calculated. The black triangle line is the case for ideal Dicke superradiance with $g^{(2)}(0) = 2 - 2/N$ as a comparison. The data of decoherence matrix for a 15-emitter system

can be found in Supplemental Material. It can be seen that $g^{(2)}(0)$ of emitters in the ENZ waveguide is close and almost parallel to the ideal Dicke superradiance. Through numerical interpolation we can calculate $g^{(2)}(0)$ when the number of atoms is uniformly increased on the central axis of the slit. When N is large enough, as shown in the inset of Fig. 2(e), $g^{(2)}(0)$ can reach about 1.9, which is very close to the maximum value of 2.

To demonstrate the similarity between the emission dynamics of emitters in ENZ waveguide and the optimal Dicke superradiance, we plot the evolution of the normalized total emission rate over time for the case of 7 emitters in Fig. 3. The black solid and the red dotted lines in the figure represent the ENZ waveguide and the optimal Dicke superradiance, respectively. It can be seen that they have very close dynamic curves and similar maximum emission rates, which shows that the superradiance in the ENZ waveguide is very close to Dicke superradiance. As a comparison, we also plot the case that emitters in vacuum and have the same spatial arrangement. In vacuum, the dissipative coupling between two emitters can be calculated as

$$\frac{\gamma_{ij}}{\gamma_0} = \frac{3}{2k_0 R} \left[\sin(k_0 R) + \frac{\cos(k_0 R)}{k_0 R} - \frac{\sin(k_0 R)}{k_0^2 R^2} \right], \quad (18)$$

where k_0 is the wavevector in vacuum, and R is the distance between two emitters. A brief derivation of the formula can be found in Supplemental Material. The calculated result is presented with a blue dashed line in Fig. 3, where we can find that, although the superradiance also occurs at such a small distance, the maximum emission rate is much smaller than in the ENZ and Dicke case.

B. Superradiance of emitters in dielectric ENZ photonic crystal

According to Sec. III A we know that a plasmonic waveguide with a near-zero index can provide long-range interactions between emitters and thus near-ideal superradiance. However, due to the large dissipation in plasmonic systems, single-emitter decay and long-range interactions are bound to be affected by dissipation in the environment. All-dielectric ENZ materials can avoid dissipation and therefore have the potential to achieve longer-distance interactions [54–57].

Here we choose a diamond cylinder square photonic crystal whose ENZ frequency is within the visible light range [57]. The unit cell of this photonic crystal is depicted in Fig. 4(a), where the lattice constant $a = 480.3$ nm, the radius of the cylinder $R = 85.3$ nm and the refractive index of the cylinder is $n = 2.41$, and the surrounding is air. The energy band diagram of the photonic crystal and the effective index of the structure can be found in Supplemental Material. Two panels of Fig. 4(b) show respectively the distribution of the electric field generated in space when an emitter is located at the center of the cylinder or the corner of the cell [see the two red stars in Fig. 4(a)]. Here we calculate the field distribution of a 71×71 cylindrical array, but in order to see the details clearly, only the 4×4 array is shown here. According to

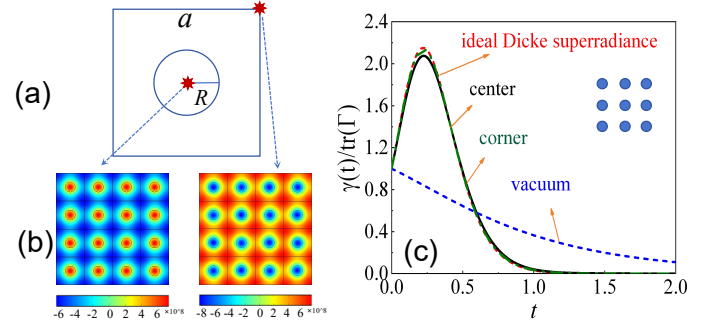


FIG. 4. (Color online) (a) The schematic diagram of photonic crystal cell. (b) Field patterns of single emitter located at the center of the cylinder and the corner of the cell, respectively. (c) Total normalized emission rate $\gamma(t)/\text{tr}(\Gamma)$ versus time t with four cases: The 9 emitters are arranged with a 3×3 array at the center of cylinders (black solid line), at the corners of cells (green dot-dashed line), ideal Dicke superradiance (red dotted line) and in the vacuum (blue dashed line). The emitters have the same spatial arrangement in three cases, as indicated in the inset.

Fig. 4(b), regardless of whether the source is at the center of the cylinder or the corner of the cell, the field distribution in the space changes periodically with the lattice. This periodic field distribution originates from the near-zero effective index. In addition, we observe that the dissipative coupling along the straight line at the corner is more uniform along the straight line at the center of the cylinder, because the electric field inside and outside the cylinder will change drastically. In other words, in order to obtain a more uniform decoherence matrix, it is better to place the emitter at the corner. Detailed information can be found in the Supplemental Material.

We calculate the decoherence matrix of 9 emitters located in the center and corner of the cylinders arranged as a 3×3 array, as shown in the inset of Fig. 4(a). The calculated data can be found in Supplemental Material. The second-order correlation can be easily calculated as $g^{(2)}(0) = 1.725$ and 1.768 , respectively, which are very close to that for an ideal case with $g^{(2)}(0) = 1.7778$. The dynamics of total emission rate in these two cases are plotted with solid black and green dot-dashed lines in Fig. 4(c), where the red dotted and blue dashed lines are the ideal Dicke superradiance and the case in vacuum, respectively.

According to Fig. 4(c), the emission dynamics of 9 emitters embedded in ENZ photonic crystal is very close to the ideal Dicke superradiance, and the superradiance even does not occur in the vacuum under the same spatial arrangement. Therefore, the ENZ photonic crystal provides a near-ideal all-to-all interaction in extended space.

IV. ROLE OF CORRELATION IN PHOTON EMISSION DYNAMIC OF ALL-INVERTED EMITTERS

In Sec. II we derived the superradiance condition using the decoherence matrix, which concerns the dynamics of emission at the early stage of the whole emission process. We now

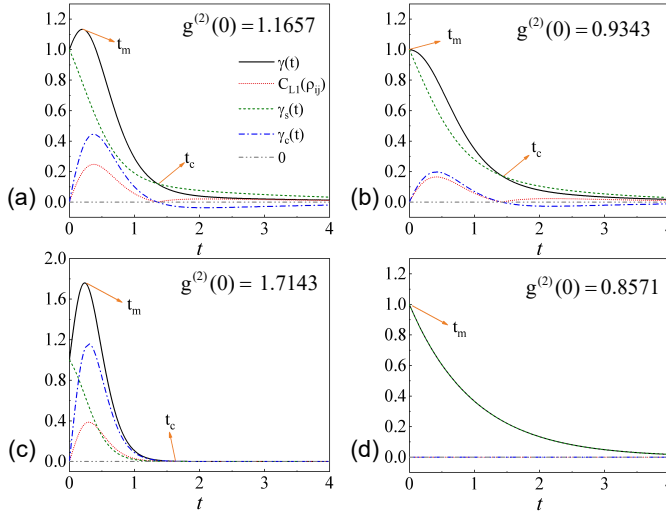


FIG. 5. (Color online) Role of correlation in emission dynamics. The black solid lines are the total emission rate $\gamma(t)$, green dashed and red dotted lines represent the single-emitter and collective emission rates $\gamma_s(t)$ and $\gamma_c(t)$, respectively. The blue dash-dotted line is the two-emitter l_1 -norm coherence C_{L1} . The gray dot-dot-dashed line is the reference zero line. The $\gamma(t)$, $\gamma_s(t)$ and $\gamma_c(t)$ are all normalized with the emitter number $N = 7$. The diagonal elements of Γ matrix are 1 and the non-diagonal elements α are taken as (a) 0.6, (b) 0.3, (c) 1.0 and (d) 0.0.

turn to consider the later emission dynamics and explore the role of correlations in the dynamics of collective emission. Note that here we use the term collective emission instead of superradiance. This is because, as we will see in this Section, the appearance of superradiance must be accompanied by collective emission, but superradiance does not necessarily occur when collective emission occurs.

It can be seen from Eq. (9) that the dissipative coupling γ_{ij} is always beneficial to the increase of the total radiation rate in the early stage of emission, but according to Eq. (7), the collective contribution $\gamma_c(t)$ may be negative (the average of $\hat{\sigma}_i^{\dagger}\hat{\sigma}_j$ at time t can be negative), which means that in the later stage of emission, correlation may be harmful to the total spontaneous radiation rate. In this case, there will be a crossover between total emission $\gamma(t)$ and single-emitter emission $\gamma_s(t)$.

We still first consider the all-to-all case, that is, the decoherence matrix is homogeneous as shown in Eq. (15). We plot the total emission rates as a function of time in Fig. 2. The number of emitters is fixed at $N = 7$, and $\alpha = 0.6, 0.3, 1.0$ and 0.0 correspond to four panels, respectively. According to Eq. (16), it is easy to calculate that $g^{(2)}(0) = 1.1657, 0.9343, 1.7143$ and 0.8571 in four cases. In four panels, the black solid lines represent the total emission rate $\gamma(t)$, the green dashed and blue dot-dashed lines represent single-emitter and collective emission parts $\gamma_s(t)$ and $\gamma_c(t)$, respectively. As marked in Fig. 5, t_m represents the time that corresponds to the maximum emission rate, and t_c is the crossover between the total decay rate $\gamma(t)$ and single-emitter decay rate $\gamma_s(t)$. If $t_m = 0$, as shown in Figs. 5(b) and 5(d), we have $g^{(2)}(0) < 1$, and there is no

superradiance. Otherwise, as shown in Figs. 5(a) and 5(c), the second-order correlation $g^{(2)}(0) > 1$, and the nonzero t_m indicate superradiance. In Fig. 5(b), during the time period from 0 to t_c , although there is no emission burst, the total spontaneous emission is still greater than the single-emitter spontaneous emission, that is, collective emission plays a positive role in the emission process. This can be demonstrated through the dynamics of the collective part of emission $\gamma_c(t)$. Figs. 5(a) and (b) present an obvious cross between the $\gamma(t)$ and $\gamma_s(t)$, where we can find that the crossover corresponds exactly to the time that $\gamma_c(t)$ turns from positive to negative. Therefore, no matter whether superradiance occurs or not, $\gamma_c(t)$ is always positive when $t < t_c$, and after t_c , the collective effect has a negative effect on the total photon emission.

Although γ_c is the collective effect caused by correlations between emitters, it is not a genuine quantum resource because it can be negative. Then it is interesting to consider the relationship between quantum resources and collective emission. Under the scenario of all-to-all interactions, all emitters have the same environment, therefore, here we use the l_1 -norm quantum coherence [58] of the reduced density matrix of any two emitters C_{L1} to measure the emitter-emitter correlation, which is equal to the sum of the modulus of the off-diagonal element

$$C_{L1}(\rho) = \sum_{i \neq j} |\rho_{ij}|, \quad (19)$$

where ρ_{ij} is the element of the two-emitter reduced density matrix ρ .

The quantum coherence in four cases is plotted with red dashed lines in Fig. 5. As shown in the four panels, within the time period from 0 to t_c , quantum coherence is always synchronous with the collective part γ_c , that is, they increase from 0, then reach the maximum, and at last decrease to 0 at the same time. But after t_c , the quantum coherence suddenly recovers from zero, which is different from γ_c that smoothly decreases to a negative value. This illustrates that non-zero quantum correlations can also be harmful to collective emission. In addition, the synchrony of quantum coherence and collective radiation provides us with a way to determine when collective radiation ends. Collective emission shown in Eq. (7) requires measurement of all emitter-emitter correlations. However, by measuring the quantum coherence between one pair of emitters, we can determine when the collective emission ends.

More importantly, according to Fig. 5, we find that the maximum value of quantum coherence C_m is strongly dependent on the second-order correlation function $g^{(2)}(0)$ and the maximum emission rate γ_m . By solving the dynamics of few-emitter systems, we extract the maximum information of quantum coherence and plot its dependence on $g^{(2)}(0)$ and γ_m in Fig. 6(a) and 6(b), respectively. According to Fig. 6(a) we find that the maximum C_m increases exponentially with the increase of $g^{(2)}(0)$ when $g^{(2)}(0)$ is small, and then increases almost linearly with $g^{(2)}(0)$. Therefore, the maximum quantum coherence can be inferred from $g^{(2)}(0)$, regardless of whether superradiance occurs or not.

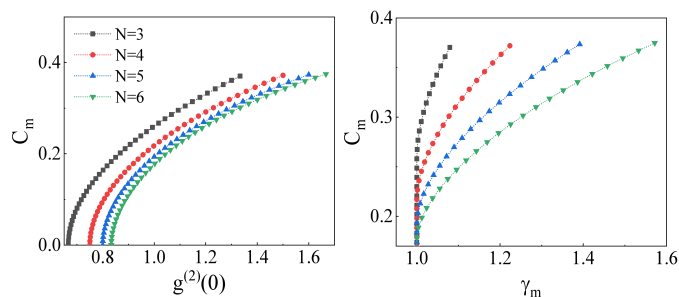


FIG. 6. (Color online) Dependence of maximum two-emitter quantum coherence C_m on the (a) second-order correlation $g^{(2)}(0)$ and (b) maximum emission rate γ_m , with different emitter numbers N .

What is more interesting is that, according to the dependence of C_m on the γ_m as shown in Fig. 6(b), when superradiance occurs, the quantum correlation in the system can be inferred just by measuring the maximum value of the total emission rate of the multi-emitter system without any quantum operator measurement. Since the measurement of total radiation intensity is direct and simple, this result provides a new suggestion for measuring the maximum value of quantum correlation in multi-emitter systems.

V. SUMMARY

Using the derived second-order correlation at initial time, we can determine whether superradiance will occur of a multi-emitter system in complex electromagnetic environment, by only dealing with the N -dimensional decoherence matrix. We investigated the superradiance properties of multi-emitter system in plasmonic ENZ waveguide and dielectric ENZ photonic crystal, where the long-range interaction can be obtained at their cut-off frequencies. It is demonstrated that, the emitters in both structures can burst light in a short time, which is very close to the ideal Dicke superradiance. This gives the near-zero-index structures great potential to achieve the ideal Dicke superradiance in extended space. By separately studying single-emitter emission and collective emission in emission dynamics in all-to-all interaction systems, we found that the quantum coherence of emitters and collective emission is highly synchronized. That is, quantum coherence is beneficial to the enhancement of the radiation rate during collective emission. But once the collective emission stops, the recovered non-zero coherence will be harmful to the emission rate. We also found that when superradiance occurs, the maximum quantum coherence and the maximum emission rate are highly correlated, thus the quantum coherence in the system can be estimated by measuring the easily accessible emission rate. The results of this work could be applied to the fields of light-matter interaction and quantum information.

ACKNOWLEDGMENTS

This work was supported by the CRF of Hong Kong (C6009-20G), the NSF-China (Grant Nos. 11575051, 11904078), and Hebei NSF (Grant Nos. A2019205266, A2021205020). JR was also funded by the project of China Postdoctoral Science Foundation (Grant No. 2020M670683).

-
- [1] R. H. Dicke, Coherence in spontaneous radiation processes, *Phys. Rev.* **93**, 99 (1954).
 - [2] N. E. Rehler and J. H. Eberly, Superradiance, *Phys. Rev. A* **3**, 1735 (1971).
 - [3] M. Gross and S. Haroche, Superradiance: An essay on the theory of collective spontaneous emission, *Phys. Rep.* **93**, 301 (1982).
 - [4] L.-M. Duan, M. D. Lukin, J. I. Cirac, and P. Zoller, Long-distance quantum communication with atomic ensembles and linear optics, *Nature* **414**, 413 (2001).
 - [5] C. W. Chou, S. V. Polyakov, A. Kuzmich, and H. J. Kimble, Single-Photon Generation from Stored Excitation in an Atomic Ensemble, *Phys. Rev. Lett.* **92**, 213601 (2004).
 - [6] R. Monshouwer, M. Abrahamsson, F. van Mourik, and R. van Grondelle, Superradiance and exciton delocalization in bacterial photosynthetic light-harvesting systems, *J. Phys. Chem. B* **101**, 7241 (1997).
 - [7] G. D. Scholes, Designing light-harvesting antenna systems based on superradiant molecular aggregates, *Chem. Phys.* **275**, 373 (2002).
 - [8] G. L. Celardo, P. Poli, L. Lussardi, and F. Borgonovi, Cooperative robustness to dephasing: Single-exciton superradiance in a nanoscale ring to model natural light-harvesting systems, *Phys. Rev. B* **90**, 085142 (2014).
 - [9] R. Reimann, W. Alt, T. Kampschulte, T. Macha, L. Ratschbacher, N. Thau, S. Yoon, and D. Meschede, Cavity-Modified Collective Rayleigh Scattering of Two Atoms, *Phys. Rev. Lett.* **114**, 023601 (2015).
 - [10] M. Hebenstreit, B. Kraus, L. Ostermann, and H. Ritsch, Subradiance via Entanglement in Atoms with Several Independent Decay Channels, *Phys. Rev. Lett.* **118**, 143602 (2017).
 - [11] P.-O. Guimond, A. Grankin, D. V. Vasilyev, B. Vermersch, and P. Zoller, Subradiant Bell States in Distant Atomic Arrays, *Phys. Rev. Lett.* **122**, 093601 (2019).
 - [12] R. G. DeVoe and R. G. Brewer, Observation of Superradiant and Subradiant Spontaneous Emission of Two Trapped Ions, *Phys. Rev. Lett.* **76**, 2049 (1996).
 - [13] J. Eschner, C. Raab, F. Schmidt-Kaler, and R. Blatt, *Nature* **413**, 495 (2001).
 - [14] Y. Kaluzny, P. Goy, M. Gross, J. M. Raimond, and S. Haroche, Observation of Self-Induced Rabi Oscillations in Two-Level Atoms Excited Inside a Resonant Cavity: The Ringing Regime of Superradiance, *Phys. Rev. Lett.* **51**, 1175 (1983).

- [15] T. Wang, S. F. Yelin, R. Cote, E. E. Eyler, S. M. Farooqi, P. L. Gould, M. Kostrun, D. Tong, and D. Vrinceanu, Superradiance in ultracold Rydberg gases, *Phys. Rev. A* **75**, 033802 (2007).
- [16] D. D. Grimes, S. L. Coy, T. J. Barnum, Y. Zhou, S. F. Yelin, and R. W. Field, Direct single-shot observation of millimeter-wave superradiance in Rydberg-Rydberg transitions, *Phys. Rev. A* **95**, 043818 (2017).
- [17] A. F. van Loo, A. Fedorov, K. Lalumière, B. C. Sanders, A. Blais, and A. Wallraff, Photon-Mediated Interactions Between Distant Artificial Atoms, *Science* **342**, 1494 (2013).
- [18] N. Lambert, Y. Matsuzaki, K. Kakuyanagi, N. Ishida, S. Saito, and F. Nori, Superradiance with an ensemble of superconducting flux qubits, *Phys. Rev. B* **94**, 224510 (2016).
- [19] Z. Wang, H. Li, W. Feng, X. Song, C. Song, W. Liu, Q. Guo, X. Zhang, H. Dong, D. Zheng, H. Wang, and D.-W. Wang, Controllable Switching between Superradiant and Subradiant States in a 10-Qubit Superconducting Circuit, *Phys. Rev. Lett.* **124**, 013601 (2020).
- [20] T. Orell, M. Zanner, M. L. Juan, A. Sharafiev, R. Albert, S. Oleschko, G. Kirchmair, and M. Silveri, Collective bosonic effects in an array of transmon devices, *Phys. Rev. A* **105**, 063701 (2022).
- [21] D. Martín-Cano, L. Martín-Moreno, F. J. García-Vidal, and E. Moreno, "Resonance energy transfer and superradiance mediated by plasmonic nanowaveguides," *Nano Lett.* **10**, 3129-3134 (2010).
- [22] V. N. Pustovit and T. V. Shahbazyan, "Plasmon-mediated superradiance near metal nanostructures," *Phys. Rev. B* **82**, 075429 (2010).
- [23] J. Ren, T. Wu, B. Yang, and X. Zhang, "Simultaneously giant enhancement of Förster resonance energy transfer rate and efficiency based on plasmonic excitations," *Phys. Rev. B* **94**, 125416 (2016).
- [24] J. de Torres, P. Ferrand, G. Colas des Francs, and J. Wenger, "Coupling emitters and silver nanowires to achieve long-range plasmon-mediated fluorescence energy transfer," *ACS Nano* **10**, 3968-3976 (2016).
- [25] J. Ren, T. Chen, B. Wang, and X. Zhang, "Ultrafast coherent energy transfer with high efficiency based on plasmonic nanostructures," *J. Chem. Phys.* **146**, 144101 (2017).
- [26] J. Ren, T. Chen, and X. Zhang, "Long-lived quantum speedup based on plasmonic hot spot systems", *New J. Phys.* **21**, 053034 (2019).
- [27] J. A. Mlynek, A. A. Abdumalikov, C. Eichler, and A. Wallraff, Observation of Dicke superradiance for two artificial atoms in a cavity with high decay rate, *Nat. Commun.* **5**, 5186 (2014).
- [28] A. Goban, C.-L. Hung, J. D. Hood, S.-P. Yu, J. A. Muniz, O. Painter, and H. J. Kimble, Superradiance for Atoms Trapped along a Photonic Crystal Waveguide, *Phys. Rev. Lett.* **115**, 063601 (2015).
- [29] S. J. Masson, I. Ferrier-Barbut, L. A. Orozco, A. Browaeys, and A. Asenjo-Garcia, Many-Body Signatures of Collective Decay in Atomic Chains, *Phys. Rev. Lett.* **125**, 263601 (2020).
- [30] S. J. Masson and A. Asenjo-Garcia, Atomic-waveguide quantum electrodynamics, *Phys. Rev. Res.* **2**, 043213 (2020).
- [31] S. Cardenas-Lopez, S. J. Masson, Z. Zager, and A. Asenjo-Garcia, Many-body superradiance and dynamical symmetry breaking in waveguide QED, *Phys. Rev. Lett.* **131**, 033605 (2023).
- [32] F. Robicheaux, Theoretical study of early-time superradiance for atom clouds and arrays, *Phys. Rev. A* **104**, 063706 (2021).
- [33] L. Ruks and T. Busch, Green's functions of and emission into discrete anisotropic and hyperbolic baths, *Phys. Rev. Res.* **4**, 023044 (2022).
- [34] O. Rubies-Bigorda and S. F. Yelin, Superradiance and subradiance in inverted atomic arrays, *Phys. Rev. A* **106**, 053717 (2022).
- [35] S. J. Masson and A. Asenjo-Garcia, Universality of Dicke superradiance in arrays of quantum emitters, *Nat. Commun.* **13**, 2285 (2022).
- [36] E. Sierra, S. J. Masson, and A. Asenjo-Garcia, Dicke superradiance in ordered lattices: Dimensionality matters, *Phys. Rev. Res.* **4**, 023207 (2022).
- [37] W.-K. Mok, A. Asenjo-Garcia, T. C. Sum, and L.-C. Kwek, Dicke Superradiance Requires Interactions beyond Nearest Neighbors, *Phys. Rev. Lett.* **130**, 213605 (2023).
- [38] H. J. Carmichael and K. Kim, A quantum trajectory unraveling of the superradiance master equation, *Opt. Commun.* **179**, 417 (2000).
- [39] J. P. Clemens, L. Horvath, B. C. Sanders, and H. J. Carmichael, Collective spontaneous emission from a line of atoms, *Phys. Rev. A* **68**, 023809 (2003).
- [40] F. Robicheaux, Theoretical study of early-time superradiance for atom clouds and arrays, *Phys. Rev. A* **104**, 063706 (2021).
- [41] F. Robicheaux and D. A. Suresh, Beyond lowest order mean-field theory for light interacting with atom arrays, *Phys. Rev. A* **104**, 023702 (2021).
- [42] R. W. Ziolkowski, "Propagation in and scattering from a matched metamaterial having a zero index of refraction," *Phys. Rev. E* **70**, 046608 (2004).
- [43] A. Alù, M. G. Silveirinha, A. Salandrino, and N. Engheta, "Epsilon-near-zero metamaterials and electromagnetic sources: Tailoring the radiation phase pattern," *Phys. Rev. B* **75**, 155410 (2007).
- [44] N. Engheta, "Pursuing near-zero response," *Science* **340**, 286-287 (2013).
- [45] R. Maas, J. Parsons, N. Engheta, and A. Polman, "Experimental realization of an epsilon-near-zero metamaterial at visible wavelengths," *Nat. Photonics* **7**, 907 (2013).
- [46] I. Liberal and N. Engheta, "Near-zero refractive index photonics," *Nat. Photonics* **11**, 149-158 (2017).
- [47] Y. Li and C. Argyropoulos, "Exceptional points and spectral singularities in active epsilon-near-zero plasmonic waveguides," *Phys. Rev. B* **99**, 075413 (2019).
- [48] S. Zhu, L.-L. Su and J. Ren, "Tunable couplings between location-insensitive emitters mediated by an epsilon-near-zero plasmonic waveguide," *Opt. Express* **31**, 28575 (2023).
- [49] H. T. Dung, L. Knöll, and D.-G. Welsch, "Resonant dipole-dipole interaction in the presence of dispersing and absorbing surroundings," *Phys. Rev. A* **66**, 063810 (2002).
- [50] A. Gonzalez-Tudela, D. Martín-Cano, E. Moreno, L. Martín-Moreno, C. Tejedor, and F. J. García-Vidal, "Entanglement of two qubits mediated by one-dimensional plasmonic waveguides," *Phys. Rev. Lett.* **106**, 020501 (2011).
- [51] P. B. Johnson and R. W. Christy, Optical constant of the noble metals, *Phys. Rev. B* **6**, 4370-4379 (1972).
- [52] A. Alù and N. Engheta, Light squeezing through arbitrarily shaped plasmonic channels and sharp bends, *Phys. Rev. B* **78**, 035440 (2008).
- [53] C. Argyropoulos, P.-Y. Chen, G. D'Aguanno, and A. Alù, Temporal soliton excitation in an epsilon-near-zero plasmonic metamaterial, *Opt. Lett.* **39**, 5566 (2014).
- [54] P. Moitra, Y. Yang, Z. Anderson, I. I. Kravchenko, D. P. Briggs, and J. Valentine, "Realization of an all-dielectric zero-index optical metamaterial," *Nat. Photonics* **7**, 791 (2013).
- [55] I. Liberal and N. Engheta, "Zero-index structures as an alternative platform for quantum optics," *Proc. Natl. Acad. Sci.* **114**, 822 (2017).

- [56] D. I. Vulis, Y. Li, O. Reshef, P. Camayd-Munoz, M. Yin, S. Kita, M. Loncar, and E. Mazur, "Monolithic CMOS-compatible zero-index metamaterials," *Opt. Express* **25**, 12381 (2017).
- [57] O. Mello, Y. Li, S. A. Camayd-Munoz, C. DeVault, M. Lobet, H. Tang, M. Loncar, and E. Mazur, "Extended many-body superradiance in diamond epsilon near-zero metamaterials," *Appl. Phys. Lett.* **120**, 061105 (2022).
- [58] T. Baumgratz, M. Cramer, and M. B. Plenio, "Quantifying Coherence," *Phys. Rev. Lett.* **113**, 140401 (2014).

SUPPLEMENTAL MATERIAL

I. The derivation of the second-order correlation by using the quantum jump operator method

In a weakly coupled environment, after using the Born-Markov and rotating-wave approximations, and tracing out the environment, the Lindblad master equation of the emitter system can be written as [26, 49, 50]

$$\frac{\partial \rho}{\partial t} = \frac{i}{\hbar} [\rho, H] + \frac{1}{2} \sum_{i,j} \gamma_{ij} \left(2\hat{\sigma}_i \rho \hat{\sigma}_j^\dagger - \rho \hat{\sigma}_i^\dagger \hat{\sigma}_j - \hat{\sigma}_i^\dagger \hat{\sigma}_j \rho \right), \quad (1)$$

where $\hat{\sigma}_i^\dagger$ and $\hat{\sigma}_i$ are the raising and lowering operators of the i th emitter, respectively. When dealing with collective spontaneous decay, it is convenient to recast the spin operators of single emitters into the collective jump operator $\{\hat{\mathcal{O}}_\nu\}$, and the Lindblad equation can be written as

$$\frac{\partial \rho}{\partial t} = \frac{i}{\hbar} [\rho, H] + \frac{1}{2} \sum_{\nu} \Gamma_{\nu} \left(2\hat{\mathcal{O}}_{\nu} \rho \hat{\mathcal{O}}_{\nu}^\dagger - \rho \hat{\mathcal{O}}_{\nu}^\dagger \hat{\mathcal{O}}_{\nu} - \hat{\mathcal{O}}_{\nu}^\dagger \hat{\mathcal{O}}_{\nu} \rho \right), \quad (2)$$

with $\{\Gamma_{\nu}\}$ being the eigenvalues of decoherence matrix $\mathbf{\Gamma}$ which has the form

$$\mathbf{\Gamma} = \begin{pmatrix} \gamma_{11} & \gamma_{12} & \cdots & \gamma_{1N} \\ \gamma_{21} & \gamma_{22} & \cdots & \gamma_{2N} \\ \vdots & \vdots & \ddots & \vdots \\ \gamma_{N1} & \gamma_{N2} & \cdots & \gamma_{NN} \end{pmatrix}, \quad (3)$$

where the dissipative coupling γ_{ij} is the dissipative coupling between the i th and j th emitters, which can be calculated using electromagnetic Green's tensor, as shown in Eq. (4) of the main text. The collective ν -jump operator $\hat{\mathcal{O}}_{\nu}$ can be written as

$$\hat{\mathcal{O}}_{\nu} = \sum_{i=1}^N \alpha_{\nu,i} \hat{\sigma}_i, \quad \hat{\mathcal{O}}_{\nu}^\dagger = \sum_{i=1}^N \alpha_{\nu,i}^* \hat{\sigma}_i^\dagger \quad (4)$$

and $(\alpha_{\nu,1}, \alpha_{\nu,2}, \dots, \alpha_{\nu,N})^T$ is the normalized eigenvector of matrix $\mathbf{\Gamma}$ corresponds to the eigenvalue Γ_{ν} , thus we have

$$\sum_{i=1}^N \alpha_{\nu,i}^* \alpha_{\mu,i} = \delta_{\nu\mu}. \quad (5)$$

In this case, the matrix elements of $\mathbf{\Gamma}$ showed in Eq. (3) is

$$\gamma_{ij} = \sum_{\nu=1}^N \Gamma_{\nu} \alpha_{\nu,i} \alpha_{\nu,j}^*, \quad (6)$$

and naturally, $\gamma_{ii} = \sum_{\nu=1}^N \Gamma_{\nu} |\alpha_{\nu,i}|^2$.

The superradiance can be captured by a second-order correlation function

$$g^{(2)}(0) = \frac{\sum_{\nu,\mu=1}^N \Gamma_{\nu} \Gamma_{\mu} \langle \hat{\mathcal{O}}_{\nu}^\dagger \hat{\mathcal{O}}_{\mu}^\dagger \hat{\mathcal{O}}_{\mu} \hat{\mathcal{O}}_{\nu} \rangle}{\left(\sum_{\nu=1}^N \Gamma_{\nu} \langle \hat{\mathcal{O}}_{\nu}^\dagger \hat{\mathcal{O}}_{\nu} \rangle \right)^2}, \quad (7)$$

where the average is taken on the fully inverted state $|e\rangle^{\otimes N}$ at the start time. Substituting the ν -jump operator showed in Eq. (4) into the formula above, we have

$$g^{(2)}(0) = \frac{\sum_{\nu,\mu=1}^N \Gamma_\nu \Gamma_\mu \sum_{i,j,l,m=1}^N \alpha_{\nu,i}^* \alpha_{\mu,j}^* \alpha_{\mu,l} \alpha_{\nu,m} \langle \hat{\sigma}_i^\dagger \hat{\sigma}_j^\dagger \hat{\sigma}_l \hat{\sigma}_m \rangle}{\left(\sum_{\nu=1}^N \Gamma_\nu \sum_{i,j=1}^N \alpha_{\nu,i}^* \alpha_{\nu,j} \langle \hat{\sigma}_i^\dagger \hat{\sigma}_j \rangle \right)^2}. \quad (8)$$

For the fully inverted initial state, we have $\langle \hat{\sigma}_i^\dagger \hat{\sigma}_j \rangle = \delta_{ij}$ and $\langle \hat{\sigma}_i^\dagger \hat{\sigma}_j^\dagger \hat{\sigma}_l \hat{\sigma}_m \rangle = (\delta_{im} \delta_{jl} + \delta_{il} \delta_{jm}) (1 - \delta_{ij})$. Therefore, the second-order correlation function is

$$\begin{aligned} g^{(2)}(0) &= \frac{\sum_{\nu,\mu=1}^N \Gamma_\nu \Gamma_\mu \left(\sum_{i,j=1}^N |\alpha_{\nu,i}|^2 |\alpha_{\mu,j}|^2 + \sum_{i,j=1}^N \alpha_{\nu,i}^* \alpha_{\mu,j}^* \alpha_{\mu,i} \alpha_{\nu,j} - 2 \sum_{i=1}^N |\alpha_{\nu,i}|^2 |\alpha_{\mu,i}|^2 \right)}{\left(\sum_{\nu=1}^N \Gamma_\nu \sum_{i=1}^N |\alpha_{\nu,i}|^2 \right)^2} \\ &= \frac{\sum_{\nu,\mu=1}^N \Gamma_\nu \Gamma_\mu \left[\left(\sum_{i=1}^N |\alpha_{\nu,i}|^2 \right) \left(\sum_{j=1}^N |\alpha_{\mu,j}|^2 \right) + \left(\sum_{i=1}^N \alpha_{\nu,i}^* \alpha_{\mu,i} \right) \left(\sum_{j=1}^N \alpha_{\mu,j}^* \alpha_{\nu,j} \right) - 2 \sum_{i=1}^N |\alpha_{\nu,i}|^2 |\alpha_{\mu,i}|^2 \right]}{\left(\sum_{\nu=1}^N \Gamma_\nu \sum_{i=1}^N |\alpha_{\nu,i}|^2 \right)^2} \\ &= \frac{\sum_{\nu,\mu=1}^N \Gamma_\nu \Gamma_\mu \left[1 + \delta_{\nu\mu} - \sum_{i=1}^N 2 |\alpha_{\nu,i}|^2 |\alpha_{\mu,i}|^2 \right]}{\left(\sum_{\nu=1}^N \Gamma_\nu \right)^2} \\ &= \frac{\sum_{\nu,\mu=1}^N \Gamma_\nu \Gamma_\mu + \sum_{\nu=1}^N \Gamma_\nu^2 - 2 \sum_{i=1}^N \left(\sum_{\nu=1}^N \Gamma_\nu |\alpha_{\nu,i}|^2 \right) \left(\sum_{\mu=1}^N \Gamma_\mu |\alpha_{\mu,i}|^2 \right)}{\left(\sum_{\nu=1}^N \Gamma_\nu \right)^2} \\ &= \frac{\sum_{\nu,\mu=1}^N \Gamma_\nu \Gamma_\mu + \sum_{\nu=1}^N \Gamma_\nu^2 - 2 \sum_{i=1}^N \gamma_{ii}^2}{\left(\sum_{\nu=1}^N \Gamma_\nu \right)^2} \\ &= \frac{(\text{Tr} \mathbf{\Gamma})^2 + \text{Tr} (\mathbf{\Gamma}^2) - 2 \text{Tr} (\mathbf{\Gamma}_d^2)}{(\text{Tr} \mathbf{\Gamma})^2}. \end{aligned} \quad (9)$$

with $\mathbf{\Gamma}_d = \text{diag}(\gamma_{11}, \gamma_{22}, \dots, \gamma_{NN})$ being the diagonal matrix of decoherence matrix $\mathbf{\Gamma}$.

II. Non-uniform field induced non-identical decays and couplings

If all the emitters are in the same electromagnetic environment, that is their spontaneous decay are identical, like γ_0 , the $g^{(2)}(0)$ can take the maximum value

$$\begin{aligned} g^{(2)}(0) &= 1 + \frac{\text{Tr}(\mathbf{\Gamma}^2)}{(\text{Tr}(\mathbf{\Gamma}))^2} - \frac{2}{N}, \\ &= 1 + \frac{1}{N} \left[\text{Var} \left(\frac{\{\Gamma_\nu\}}{\gamma_0} \right) - 1 \right], \end{aligned} \quad (10)$$

which is the same to the existing results [nc,prl23], where the free-space condition is assumed. According to Eq. (10), the superradiance condition $g^{(2)}(0) > 1$ corresponds to the variance of $\{\Gamma_\nu\}/\gamma_0$ is larger than 1. From the perspective of emitting photons, large variance means that a large number of ν -jump channels are closed, that is, most collective emission modes are dark modes, while the emitter system radiates photons in burst through a small number of collective channels (bright channels).

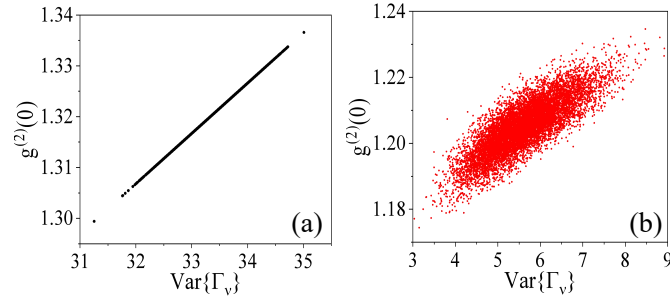


FIG. 1. (Color online) The second-order correlation $g^{(2)}(0)$ versus variance of eigenvalues of decoherence matrix $\text{Var}\{\Gamma_\nu\}$ for (a) identical and (b) different single-emitter emission rates. The number of emitter is $N=1000$ and the results of 10000 random decoherence matrices are presented in both panels.

As indicated in Eq. (10), when the single emitter emission rate is identity, the $g^{(2)}(0)$ is proportional to the variance of the eigenvalues of matrix Γ for a fixed emitter number N . However, when the decay rates of emitters are no longer equal, the $g^{(2)}(0)$ must be calculated using Eq. (9). Here we want to visually show that Eq. (10) no longer holds in this case.

In Fig. 1, we plot the relationship between $g^{(2)}(0)$ showed in Eq. (10) and the variance of eigenvalues of decoherence matrix $\text{Var}\{\Gamma_\nu\}$ by taking 10000 random decoherence matrix Γ for the two cases. The dimension of the decoherence matrix Γ (namely the number of the emitters) is fixed at $N = 1000$. In Fig. 1(a) all the diagonal elements of Γ is taken as unity, and the other elements are random numbers range from 0 to 1. While for Fig. 1(b) all the matrix elements are taken randomly from 0 to 1, other than that the condition $\gamma_{ij} \leq \min\{\gamma_{ii}, \gamma_{jj}\}$. According to Fig. 1(a), $g^{(2)}(0)$ is indeed proportional to $\text{Var}\{\Gamma_\nu\}$ when single-emitter emission rates are equal. But this relationship is broken when single-emitter emission rates are not equal, as shown in Fig. 1(b).

Now we verify the sufficiency and necessity of the minimal superradiance condition, by calculating the emission dynamics of random-coupled few-emitter system.

III. The Green's tensor profile of incoherent coupling of two emitters in homogeneous medium

The compact form of dyadic Green's function in the homogeneous medium is

$$\overset{\leftrightarrow}{G}(\vec{r}_i, \vec{r}_j, \omega) = \left[\overset{\leftrightarrow}{I} + \frac{1}{k^2} \nabla \nabla \right] \frac{e^{ik|\vec{r}_i - \vec{r}_j|}}{4\pi|\vec{r}_i - \vec{r}_j|}, \quad (11)$$

where

$$\nabla = \frac{\partial}{\partial x} \hat{x} + \frac{\partial}{\partial y} \hat{y} + \frac{\partial}{\partial z} \hat{z}, \quad (12)$$

and after some calculations its explicit form can be expresses as

$$\overset{\leftrightarrow}{G}(\vec{r}_i, \vec{r}_j, \omega) = \left\{ \left(\frac{3}{k^2 R^2} - \frac{3i}{kR} - 1 \right) \hat{R} \hat{R} + \left(1 + \frac{i}{kR} - \frac{1}{k^2 R^2} \right) \overset{\leftrightarrow}{I} \right\} \frac{e^{ikR}}{4\pi R}, \quad (13)$$

with $R = |\vec{r}_i - \vec{r}_j|$, and $\hat{R} = (\vec{r}_i - \vec{r}_j)/|\vec{r}_i - \vec{r}_j|$.

If the electric dipole moments of two emitters are parallel and perpendicular to the line connecting their positions (that is, perpendicular to \hat{R}), then the dissipative interaction between then can be calculated as

$$\begin{aligned} \gamma_{ij} &= \frac{2\omega_0^2}{\varepsilon_0 \hbar c^2} \text{Im} \left[\vec{\mu}_i^* \cdot \overset{\leftrightarrow}{G}(\vec{r}_i, \vec{r}_j, \omega) \cdot \vec{\mu}_j \right] \\ &= \frac{2\omega_0^2}{\varepsilon_0 \hbar c^2} \text{Im} \left[1 + \frac{i}{kR} - \frac{1}{k^2 R^2} \right] \frac{e^{ikR}}{4\pi R} \\ &= \frac{2\omega_0^2}{\varepsilon_0 \hbar c^2} \mu^2 \frac{1}{4\pi R} \left[\sin(kR) + \frac{\cos(kR)}{kR} - \frac{\sin(kR)}{k^2 R^2} \right]. \end{aligned} \quad (14)$$

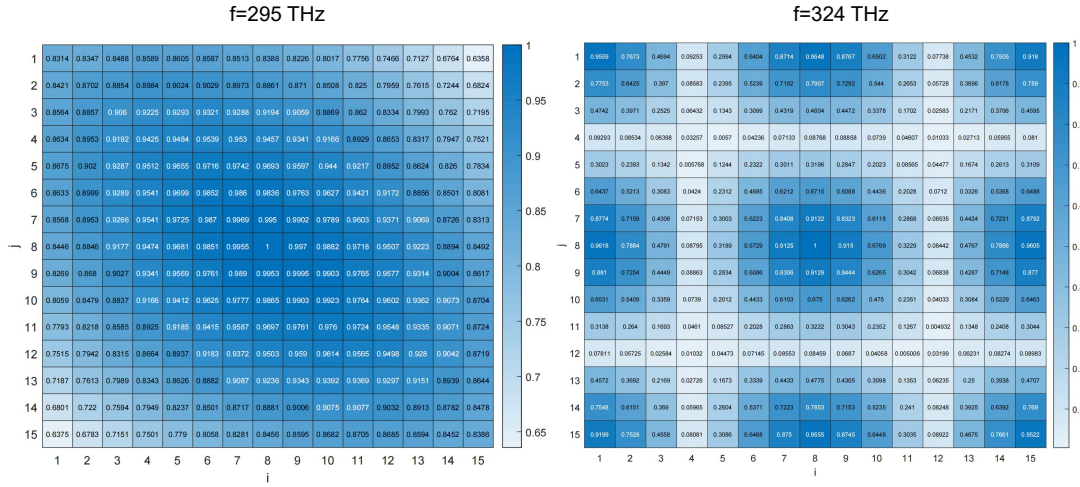


FIG. 2. (Color online) The calculated decoherence matrix Γ of 15 emitters uniformly located on the central line of the slit waveguide. The transition frequency of the emitters are taken as (left panel) $f = 295$ THz that is the cutoff frequency that ENZ occurs, and (right panel) $f = 324$ THz which is another resonance frequency but not ENZ.

The decay rate of an emitter in the homogeneous medium is

$$\gamma_{ii} = n \left(\frac{\omega^3 \mu^2}{3\pi \epsilon_0 \hbar c^3} \right) = n \gamma_0, \quad (15)$$

where $\gamma_0 = k_0^3 \mu^2 / (3\pi \epsilon_0 \hbar)$ is the spontaneous of single emitter in vacuum, $k_0 = \omega/c$ is the wavevector in vacuum, and n is the refractive index of the homogeneous medium. Therefore, in a homogeneous medium we have the normalized dissipative coupling

$$\frac{\gamma_{ij}}{\gamma_{ii}} = \frac{3}{2n k_0 R} \left[\sin(kR) + \frac{\cos(kR)}{kR} - \frac{\sin(kR)}{k^2 R^2} \right], \quad (16)$$

and in the vacuum,

$$\frac{\gamma_{ij}}{\gamma_0} = \frac{3}{2k_0 R} \left[\sin(k_0 R) + \frac{\cos(k_0 R)}{k_0 R} - \frac{\sin(k_0 R)}{k_0^2 R^2} \right]. \quad (17)$$

IV. Data of decoherence matrix of emitter in ENZ waveguide and photonic crystal

In Fig. 2, we plot the heatmap of the calculated decoherence matrix Γ of 15 emitters uniformly located on the central line of the slit waveguide. The transition frequency of the emitters are taken as (a) $f = 295$ THz that is the cutoff frequency that ENZ occurs, and (b) $f = 324$ THz which is another resonance frequency but not ENZ. Obviously, in the case of ENZ, the coupling changes gradually with the emitter-emitter distance, while at the non-ENZ resonance frequency, the coupling changes with the distance very drastically.

V. Details of ENZ photonic crystal

The photonic energy band of the 2D square cylinder photonic crystal is plotted in Fig. 3. The radius of the cylinder $R = 85.3$ nm and the refractive index of the cylinder is $n = 2.41$, and the surrounding is air. Fig. 3(b) is the calculated refractive index of photonic crystal around the frequency $f = 407.1$ THz, as marked with red dotted circles in two panels. The effective index is calculated using the boundary-mode analysis of RF module in COMSOL multiphysics.

In Fig. 3(c), we present the normalized dissipative coupling between two emitters γ_{12}/γ_{11} as a function of their separation distance d , where the first emitter is fixed at the center of a cylinder (who serves as the source when calculate the field) and the other emitter moves away from the fixed one, see the upper panel plotted with blue line. The lower panel of Fig. 3(c) is the case for the source emitter is fixed at the cell corner, and the other emitter moves along the line of cell corner. Obviously, the coupling

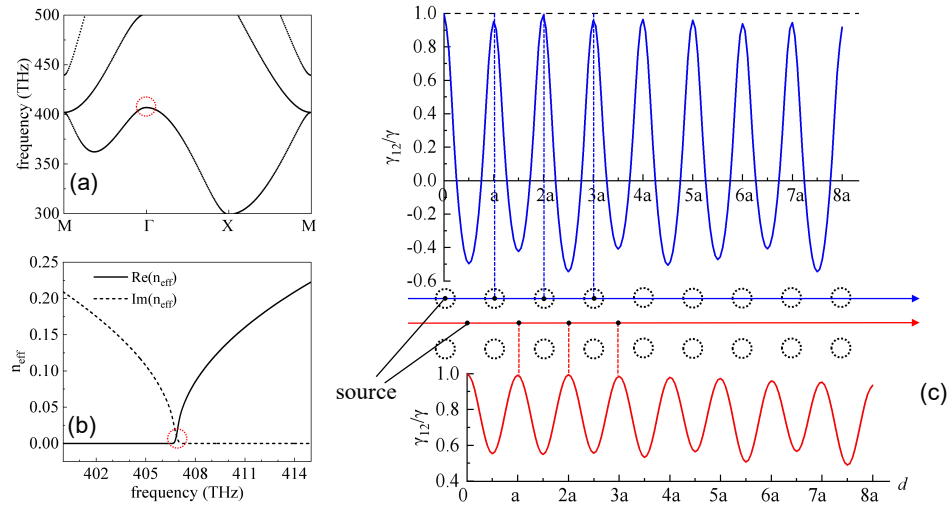


FIG. 3. (Color online) (a) The photonic energy band of the 2D square cylinder photonic crystal, the lattice constant $a = 480.3$ nm. The radius of the cylinder $R = 85.3$ nm and the refractive index of the cylinder is $n = 2.41$, and the surrounding is air. (b) The calculated refractive index of photonic crystal around the frequency $f = 407.1$ THz, as marked with red dotted circles in two panels. (c) The normalized dissipative coupling between two emitters, where an emitter is fixed at the center of a cylinder and the other emitter moves away from the fixed one, see the upper panel plotted with blue line. The case for the line along the cell corner is plotted with red line in the lower panel.

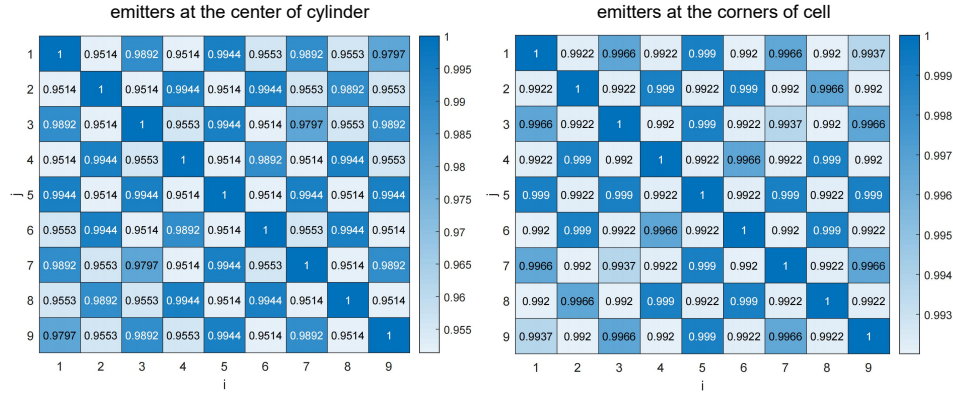


FIG. 4. (Color online) The calculated decoherence matrix Γ of 9 emitters arranged as a 3×3 two-dimensional array. All the emitters are at (left panel) the center of the cylinder, and (right panel) the corner of the cell.

of emitter in the case of the upper panel has a larger oscillating with the distance compared with the lower case. Therefore, in order to keep the coupling as uniform as possible, placing the emitter in the air rather than in the cylinder will have less stringent requirements on the position of the emitters.

Figure 4 shows the calculated decoherence matrix Γ of 9 emitters arranged as a 3×3 two-dimensional array, as shown in the inset of Fig. 4(c) of the main text. The left panel of Fig. 4 is the case that emitters located at the center of the cylinders, and the right panel represent the case that emitters are at the corners of the cells.